Multi-Beam Analysis of Satellite Swarm-Based Antenna Arrays for 6G Direct-to-Cell Connectivity

Diego Tuzi *, Thomas Delamotte *, Maik Röper †, Alea Schröder †, Bho Matthiesen †, Andreas Knopp *
*Institute of Information Technology, University of the Bundeswehr Munich, 85579 Neubiberg Germany
Email: paper.sp@unibw.de, {name.surname}@unibw.de
†Gauss-Olbers Center, c/o University of Bremen, Dept. of Communications Engineering, 28359 Bremen, Germany
Email: {surname}@ant.uni-bremen.de

***Abstract*—Non-terrestrial networks (NTNs), particularly satellite networks, are key factors for ubiquitous connectivity in today's 5G terrestrial networks (TNs) and future 6G networks. They can bring great benefits, but also great challenges. The direct-to-cell (D2C) connectivity use case, i.e., direct connectivity from satellites to common terrestrial low-gain user terminals (UTs), such as handheld or IoT devices, is currently gaining strong interest. This paper focuses on innovative distributed implementations of the space segment using swarms of multiple small platforms, each embedding one or a subset of radiating elements. They are organized with regular or irregular geometries and greater distance between radiating elements, creating large virtual antenna array apertures. The use of small satellites promises reduced production and launch costs, while the distributed nature of the system provides attractive features, such as scalability and fault tolerance. This paper analyzes the multi-beam performance of two distributed implementations, comparing the results with a single platform implementation. Distributed implementations present a better performance in terms of average summed throughput, user throughput, and throughput density. An analysis of worst-case user throughput reveals that distributed implementations based on irregular geometries capable of mitigating grating lobes provide slightly lower average performance of measured key performance indicators (KPIs), but greater fairness than the implementation based on regular geometries. Swarm-based antenna arrays appear as a promising solution for the D2C connectivity use case.**

***Index Terms*—6G, non-terrestrial network (NTN), distributed satellite system (DSS), satellite swarm, CubeSat, phased antenna array, ELSA.**

I. Introduction

Academia, industry, and standardization bodies are paving the way for the next generation of communication networks, 6G. Although there are different visions, all of them are considering as a fundamental requirement, the ubiquitous connectivity. For this reason, the integration between terrestrial networks (TNs) and non-terrestrial networks (NTNs) is a key enabler of 6G [1]. NTNs comprise multiple layers, but satellite networks definitely represent the most important one to achieve global coverage. The direct-to-cell (D2C) connectivity, i.e., direct connectivity from satellites to common terrestrial low-gain user terminals (UTs), such as handheld or Internet of things (IoT) devices, is a use case of great interest. Low-frequency bands (UHF/L/S), low Earth orbit (LEO) constellations, and new space segment architectures are mandatory building blocks to achieve the target link budget and limit the performance gap with TNs [2]. Previous LEO constellations, such as Iridium or Globalstar, can only provide limited services, such as the emergency service available on Apple smartphones. Big firms and new companies are entering the D2C business by proposing different approaches, such as the joint venture between Starlink and T-Mobile, Lynk Global, and AST SpaceMobile [3]. Despite the trend towards larger satellite antenna aperture, which brings with it new mechanical challenges and increased production and launch costs, current plans promise low data rate or basic two-way services that are far from the requirements of current and future mobile generation networks. For these reasons, the space segment needs to be redesigned to enhance the performance of NTNs.

The current technological trend for LEO satellite antennas uses direct radiating array (DRA) architectures based on phased antenna array solutions, in which the radiating elements are usually organized in a regular geometry (e.g. rectangular) spaced by a uniform distance, usually around half the wavelength (*classical implementation*). This paper is based on an alternative distributed satellite system (DSS) configuration. The classical implementation is decomposed in a swarm of multiple small platforms (e.g. CubeSats), each equipped with one or a small number of radiating elements, spaced much more than half the wavelength to create a large virtual aperture. Swarm platforms are connected using a wireless or wired connection and coordinated to achieve the coherent transmission and reception of signals (*distributed implementation*). The use of small satellites promises cost reduction for production and launch. In addition, the distributed nature of the system provides interesting features, such as scalability and fault tolerance. The benefits of swarms for D2C are also envisioned in [4]. Numerous research and space flight demonstrations have been conducted on DSS for different fields of application like astronomy, deep-space communications, meteorology, and environmental uses [5]. Most missions have been conducted with a limited number of

This research paper was funded in part by dtec.bw – Digitalization and Technology Research Center of the Bundeswehr. dtec.bw is funded by the European Union – NextGenerationEU. Furthermore, this work was partly funded by the German Ministry of Education and Research (BMBF) under grant 16KISK016 (Open6GHub) and was supported in part by European Space Agency (ESA) within the SatNExV activity WI Y2.2-A (Grant No: 4000130962/20/NL/NL/FE). The opinions and conclusions presented herein are those of the authors and can in no way be taken to reflect the official opinion of the European Space Agency.

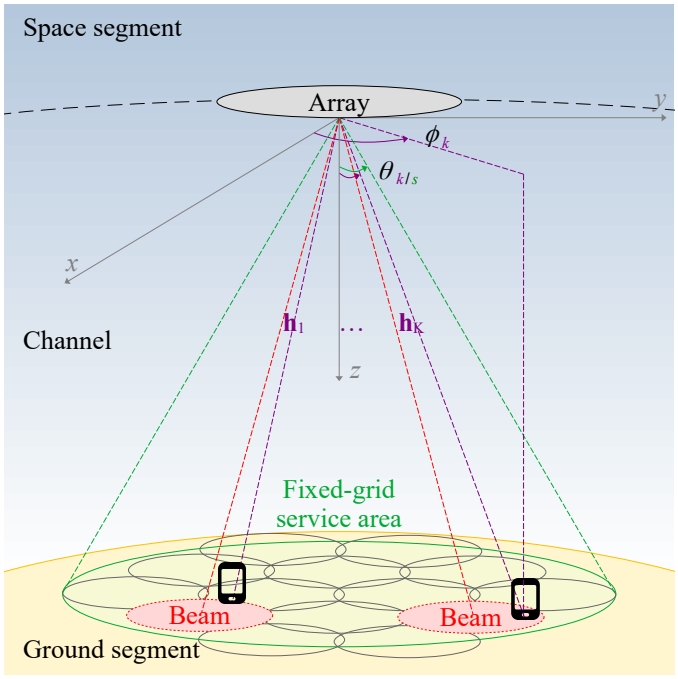

Fig. 1. High-level representation of a Massive/Multi-User MIMO downlink scenario with beamforming capabilities.

satellites, but in recent decades research has been considering systems with an increasing number of satellites, especially with the advent of small satellites [6], [7]. Swarms have also been considered in unmanned aerial vehicles (UAVs) [8] and for beaming solar power to Earth from Space [9]. DSS configurations for communication purposes have been recently considered in [10]–[12] but using higher frequencies and more powerful UTs. A DSS cluster configuration for D2C constellations is proposed in [13] while a formation of arrays for D2C considering geostationary Earth orbit (GEO) and LEO scenarios is proposed in [14]. The single beam performance of swarm-based antenna arrays has been addressed in [15], [16], where the role of geometries in large virtual antenna apertures for grating lobe mitigation has been investigated. The work in [16] also addressed the main challenges of satellite swarms for D2C. Synchronization and formation-keeping strategies (formation flying) emerged as important aspects together with the need to attest the potential of swarms in multi-beam scenarios.

This paper focuses on the multi-beam analysis of satellite swarm-based antenna arrays for D2C connectivity in 6G NTNs under the assumption of perfect synchronization and a stable swarm formation flying. The classical implementation (single platform) is compared with two different distributed implementations (swarms) using the same number of radiating elements and the same total transmitted power. It is also emphasized that distributed implementations overcome the classical implementations in terms of summed throughput, user throughput, and throughput density. A distributed implementation capable of mitigating the grating lobes provides as well a fairer allocation of resources.

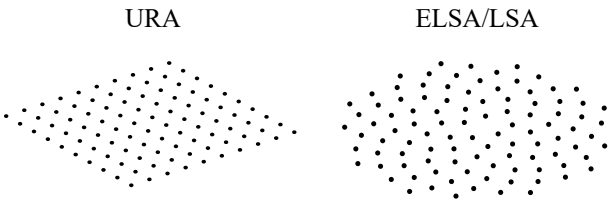

Fig. 2. Array geometries considered in the analysis, URA commonly used in classical implementations and ELSA particularly suitable for distributed implementations due to the grating lobes mitigation capability [16].

The rest of the paper is organized in three sections. Section II describes the system model, the beamforming method, the user scheduling, and the key performance indicators (KPIs). Section III presents the system parameters and the simulation results. Finally, Section IV states the conclusion and an outlook on future works.

II. System model, beamforming and KPIs

A. System model

The high-level representation of the system under analysis is shown in Fig. 1. A Massive/Multi-User MIMO downlink scenario with beamforming at the space segment is considered. The space segment is composed of an array with N radiating elements providing communication on its defined service area on the ground. The service area is limited by the maximum scan angle θ_s and it is subdivided into a fixed-grid of N_c cells. The array can generate multiple beams, each pointing to a cell center to cover the cell area and using the whole bandwidth, i.e., full frequency reuse (FFR) is assumed. The system considers the user set $\mathcal{U}$ of U single antenna UTs distributed in the service area. In a given time slot, a scheduling algorithm maps a subset of $K \leq U$ users in $\mathcal{U}$ such that each user of this subset is associated with a different cell/beam among the possible N_c cells/beams of the fixed-grid. Therefore, it is assumed that users assigned to the same cell/beam are multiplexed in a time frame with multiple slots. The k-th UT position on the ground is identified by the couple (θ_k, ϕ_k), representing the signal angle of departure (AoD) from the array center in space to the respective position on the ground.

The symbol vector $\mathbf{x} \in \mathbb{C}^{(K\times 1)}$ is transmitted over a line-of-sight (LOS) channel under clear sky conditions described by the far-field complex baseband channel matrix $\mathbf{H} = [\mathbf{h}_1, ..., \mathbf{h}_K]^T \in \mathbb{C}^{(K\times N)}$, where $\mathbf{h}_k = [h_{k,1}, ..., h_{k,N}]^T \in \mathbb{C}^{(N\times 1)}$ contains the channel coefficients between the N radiating elements and the k-th scheduled UT. Beams are generated via a beamforming/precoding operation described by the matrix $\mathbf{W} = [\mathbf{w}_1, ..., \mathbf{w}_K] \in \mathbb{C}^{(N\times K)}$ with $\mathbf{w}_k = [w_{k,1}, ..., w_{k,N}]^T \in \mathbb{C}^{(N\times 1)}$. The received signal vector $\mathbf{y} \in \mathbb{C}^{(K\times 1)}$ on the ground can be written as

$$\mathbf{y} = \mathbf{H}\,\mathbf{W}\,\mathbf{x} + \mathbf{n}, \tag{1}$$

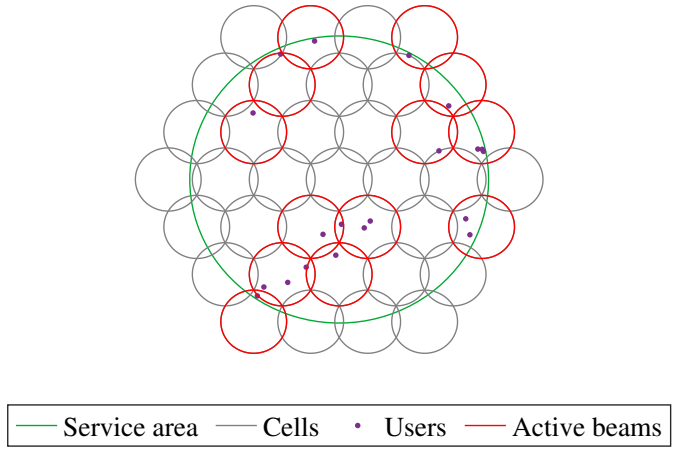

Fig. 3. Example of an operational scenario in which U=20 users are distributed within the service area. Users are mapped into K=13 cells of the fixed-grid with the smallest quadratic distance between the user's position and the center of the cell.

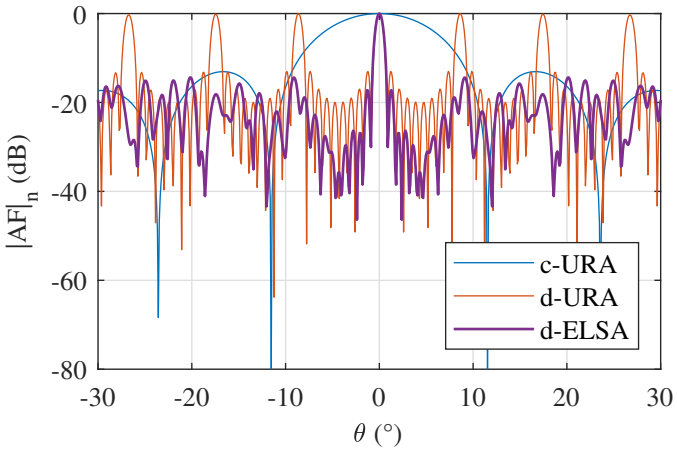

Fig. 4. Comparison of the normalized array factor between a classical implementation of the space segment using the URA geometry and two distributed implementations using URA and ELSA [16] geometry respectively.

where $\mathbf{n} \in \mathbb{C}^{(K\times 1)}$ denotes the vector with K samples of circularly symmetric additive white Gaussian noise (AWGN) having zero mean and unitary variance (due to the presence of the noise power as scaling factor in the channel definition), i.e., $\mathcal{CN}(0,1)$.

1) Space segment: The array of N radiating elements in the space segment operates in LEO, UHF/L/S frequency band, and with a limited available power. The radiating elements are considered identical with beam pattern $g^{(\mathrm{el,tx})}(\theta_k)$ and maximum gain $G_{\max}^{(\mathrm{el,tx})}$ as in [17]. The array can be implemented in two different ways:

Classical implementation (c-) embeds the N radiating elements on a single platform. It represents a phased antenna array with regular geometry and a common inter-element distance, typically $d \approx \frac{\lambda_c}{2}$, where λ_c is the wavelength of the carrier signal;

Distributed implementation (d-) considers multiple small platforms each embedding one or a subset of radiating elements (this analysis focuses on the case where each radiating element is installed on a separate platform). Platforms can be organized in a regular or irregular geometry but with a large inter-element distance $d \gg \frac{\lambda_c}{2}$.

In this paper, the classical implementation of the array considers only the URA geometry, while distributed implementations consider URA and ELSA geometries. Fig. 2 shows the two geometries. The analyzed URA is a square geometry of $\sqrt{N} \times \sqrt{N}$ radiating elements with uniform inter-element distance, and N a square number. The ELSA is a family of array geometry defined in [15], [16] based on the initial concept from [18], [19] using the Fermat's spiral. The particular ELSA geometry considered in this work is equivalent to the logarithmic spiral array (LSA) defined in [18].

2) Ground segment: The service area is subdivided into a fixed-grid of N_c cells starting from a hexagonal lattice. This is a common engineering practice to simplify the planning and design of a cellular system because the hexagon approaches a circular shape that is the ideal power coverage area [20]. The radius of the cells inside the fixed-grid is based on the average half-power beam width (HPBW) of the space segment array in the defined service area. Different array implementations have different grids.

The user set $\mathcal{U}$ is uniformly generated inside the service area, assumed to be circular, using the disk point picking method described in [21]. The users are handheld devices, i.e. smartphones, or industrial IoT devices. Each user embeds a single low-performance omnidirectional antenna with gain G^{rx}. Fig. 3 shows an illustrative circular service area with the fixed-grid of cells (continuous gray circles), and several users.

3) Channel model: The channel model considers the presence of the LOS component in a clear sky condition. The channel vector (normalized to the noise power) is

$$\mathbf{h}_k = \frac{g^{(\mathrm{el,tx})}(\theta_k)\,\mathbf{a}_k(\theta_k,\phi_k)\,G^{\mathrm{rx}}\,L^{\mathrm{fs}}(\theta_k)}{\sqrt{\kappa\,B\,T^{\mathrm{rx}}}}\,\mathrm{e}^{-j2\pi\frac{r(\theta_k)}{\lambda_c}} \tag{2}$$

where $\mathbf{a}_k(\theta_k,\phi_k)$ is the array steering vector associated with the array geometry computed at the UT position. The free-space attenuation is defined as $L^{\mathrm{fs}}(\theta_k) = \frac{\lambda_c}{4\pi r(\theta_k)}$. The value $r(\theta_k)$ is the slant range between the generic k-th UT position on the ground and the array reference system center in the space segment. The noise power is calculated considering the Boltzmann constant κ, the UT noise temperature T^{rx}, and the bandwidth of the transmitted signal B.

B. Beamforming and user scheduling

Considering the system model defined above, it is possible to delve into the operational aspects of the system, particularly the method considered for generating multiple beams and the association between users and beams.

1) Beamforming: The beamforming strategy considered is based on the maximum-ratio transmission (MRT) [22], and expressed as

$$\mathbf{W} = \sqrt{\frac{NP_{\max}^{(\mathrm{el,tx})}}{K}} \cdot \mathbf{A}^{\mathrm{b}} \in \mathbb{C}^{(N\times K)}. \tag{3}$$

TABLE I
ARRAY IMPLEMENTATIONS PARAMETERS

Array	d^{avg}	A_{e}	HPBW$^{\text{avg}}$	$r_{\text{c}}^{\text{avg}}$	N_{c}
c-URA	$0.50\lambda_{\text{c}}$	$\approx 0.4\,\text{m}^2$	$\approx 10.7°$	$\approx 47\,\text{km}$	7
d-URA	$6.67\lambda_{\text{c}}$	$\approx 67.8\,\text{m}^2$	$\approx 0.78°$	$\approx 3.4\,\text{km}$	837
d-ELSA	$6.67\lambda_{\text{c}}$	$\approx 83.7\,\text{m}^2$	$\approx 0.84°$	$\approx 3.7\,\text{km}$	745

The array steering matrix $\mathbf{A}^{\text{b}} = \left[\mathbf{a}_1^{\text{b}}, ..., \mathbf{a}_K^{\text{b}}\right] \in \mathbb{C}^{(N \times K)}$ collects the array steering vectors, where $\mathbf{a}_k^{\text{b}}$ is calculated by considering the central position of the k-th active beam on the ground and $\|\mathbf{a}_k^{\text{b}}\|_2 = 1$. The multiplicative scalar on the left side of (3) represents the square root value of the ratio of the maximum transmission power to the number of active beams. The total power of the array is calculated as the product of the number of radiating elements (N) and the power per radiating element ($P_{\max}^{(\text{el,tx})}$). More active beams reduce the power per beam but increase the spatial multiplexing gain. On the other hand, less active beams are more advantageous in terms of power per beam. Furthermore, the design of the matrix $\mathbf{W}$ takes into account the per-antenna power constraint (PAPC) [23], ensuring that each radiating element does not exceed the available power, a mandatory requirement, especially for the distributed implementation of the space segment.

2) User scheduling: A low-complexity approach is considered for user scheduling following the pragmatic approach described in [24]. Firstly, U users of the user set $\mathcal{U}$ are assigned to the K cells of the fixed-grid with the smallest quadratic distance between the user position and the center of the cell. Secondly, the array in the space segment activates K beams directed at the center positions of the cells with assigned users. However, in each time slot, only K users can be served. Therefore, it is assumed that users assigned to the same cell/beam are multiplexed in a time frame with multiple slots. The value N_k^{u} represents the number of users multiplexed over the considered time frame on the same k-th cell/beam. Fig. 3 shows an example where K=13 beams (dashed red circles) are activated to serve U=20 users distributed in the service area (purple dots). Users assigned to the same beam share the available resources equally over time.

C. KPIs

In the developed system model, the signal-to-interference-plus-noise ratio (SINR) of the scheduled k-th UT is

$$\text{SINR}_k = \frac{|\mathbf{h}_k^T \mathbf{w}_k|^2}{1 + \sum_{k' \neq k} |\mathbf{h}_k^T \mathbf{w}_{k'}|^2}. \tag{4}$$

The channel capacity per UT can be calculated using the truncated Shannon formula used by 3GPP in several technical reports. The expression adapted for the defined system is

$$C_k = \begin{cases} \frac{1}{N_k^{\text{u}}} \alpha B \log_2(1 + \text{SINR}_{\max}) & \text{SINR}_k > \text{SINR}_{\max} \\ 0 & \text{SINR}_k < \text{SINR}_{\min} \\ \frac{1}{N_k^{\text{u}}} \alpha B \log_2(1 + \text{SINR}_k) & \text{otherwise}, \end{cases} \tag{5}$$

TABLE II
SYSTEM PARAMETERS

Description	Parameter	Value
Number of Monte Carlo runs	N_{mc}	1000
Number of elements	N	100
Element max gain	$G_{\max}^{(\text{el,tx})}$	5 dBi
Element max power	$P_{\max}^{(\text{el,tx})}$	0.35 W
LEO altitude	h^{LEO}	500 km
Max scan angles	θ_s	$[-10°, 10°]$
DL center frequency	f_{c}	2.185 GHz
DL bandwidth	B	30 MHz
DL wavelength	λ_{c}	0.137 m
UT antenna gain	G^{rx}	0 dBi
UT noise temperature	T^{rx}	290 K

where $\text{SINR}_{\min} = -10\,\text{dB}$, $\text{SINR}_{\max} = 30\,\text{dB}$, and the implementation loss coefficient $\alpha = 0.6$. These choices represent baseline link level performance parameters for the 5G new radio (NR). Moreover, the normalization by $\frac{1}{N_k^{\text{u}}}$ is necessary since k-th user shares the beam with other N_k^{u} users multiplexed over the considered time frame.

Based on (5) the system performance is evaluated in terms of:

- Average sum throughput $T_{\text{sum}}^{\text{avg}}$ (Mbps): sum of the channel capacity of all the links between the array and users;
- Average user throughput $T_{\text{user}}^{\text{avg}}$ (Mbps): the ratio between the summed throughput and the number of active users;
- Worst-case user throughput $T_{\text{user}}^{\text{worst}}$ (Mbps): lowest throughput among all users. It can be considered a fairness metric of the system;
- Average throughput density $T_{\text{density}}^{\text{avg}}$ (Mbps/km^2): the ratio between the summed throughput and the total area covered by the HPBW of active beams.

III. MULTI-BEAM ANALYSIS

A. System parameters

The considered space segment operates at a LEO altitude $h^{\text{LEO}} = 500\,\text{km}$ and with a service area defined by a scan angle range $\theta_s \in [-10°, 10°]$. Distributed implementations assume a swarm of 1U CubeSats each embedding one radiating element. These kinds of platforms generally have 0.7 W of available power [25]. It is assumed that 50 % of the available power can be used to feed the radiating element. Therefore, the transmission power per radiating element is limited to $P_{\max}^{(\text{el,tx})} = 0.35\,\text{W}$. The single radiating element is considered to be a wideband CubeSat antenna with maximum gain $G_{\max}^{(\text{el,tx})} = 5\,\text{dBi}$. In terms of spectrum, the system operates at center frequency $f_{\text{c}} = 2.185\,\text{GHz}$ and bandwidth $B = 30\,\text{MHz}$ according to the downlink NTN satellite band n256 specified in [26].

The analysis considers three implementations of the array. A classical implementation with a regular URA geometry (c-URA) and conventional inter-element distance $d = \frac{\lambda_{\text{c}}}{2}$ (approximately 7 cm at the selected frequency) and two distributed implementations with inter-element distance of $d = 6.67\,\lambda_{\text{c}}$ (approximately 1 m at the selected frequency). The

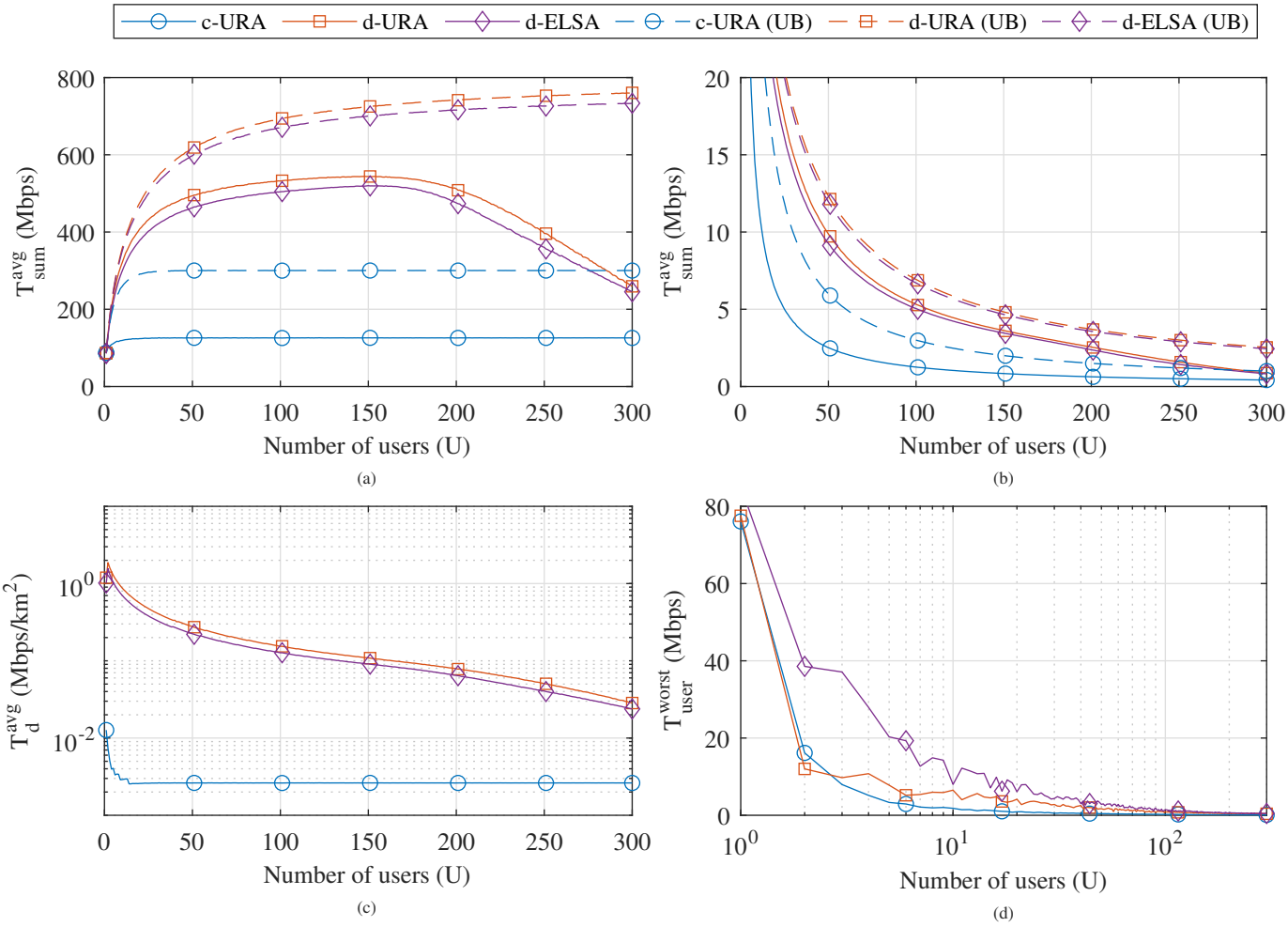

Fig. 5. Simulation results comparison of the c-URA, d-URA, and d-ELSA in terms of average sum throughput (a), average user throughput (b), worst-case user throughput (c), and average throughput density (d). Distributed implementations overcome the classical one.

first distributed implementation considers the URA geometry (d-URA), while the second considers the ELSA geometry (d-ELSA). All three array implementations use $N = 100$ radiating elements. Table I collects the parameters of the three array implementations under analysis, where A_e represents the equivalent antenna aperture, and HPBW^{avg} the average HPBW of the specific array implementation in the defined service area. Distributed implementations, thanks to their increased virtual antenna aperture, can generate narrower beams. Fig. 4 shows a 2D cut on $\phi_k = 0$ of the normalized array factor for the three different implementations. As already shown in [16], the ELSA geometry can mitigate the grating lobes present in large-spaced regular geometries. Starting from the HPBW and with simple geometrical considerations, the average cell radius r_c^{avg} can be derived (Table I). Consequently, the fixed-grid of cells can be defined based on the hexagonal pattern, as in the example in Fig. 3. In addition, the UTs are handheld or IoT devices with an omnidirectional antenna pattern and gain $G^{rx} = 0\,\text{dBi}$. Table II summarizes the main system parameters.

B. Simulation results

The system has been numerically evaluated via $N_{mc} = 1000$ Monte Carlo trials. Fig. 5 show the results in terms of the KPIs defined in Section II-C. The continuous lines were calculated considering the truncated Shannon channel capacity in (5) while the dashed lines represent the ideal best upper bound of the performance computed neglecting the impact of the inter-beam interference. It can be seen as a genie beamforming technique capable of rejecting, for each beam, all the interference generated by the other beams.

Fig. 5(a) shows the comparison in terms of average summed throughput when increasing the number of users in the system. Firstly, distributed implementations outperform the classical implementation in all the simulated conditions, because they can activate more beams in the service area. As shown in Table I, distributed implementations have hundreds of possible non-overlapping cells whereas the classical one generates only a few beams. Secondly, the performance of the distributed implementations decreases if the number of users becomes too high, due to the increased interference coming from the

other beams and the reduced power per beam. Thirdly, the performance of the classical implementation becomes constant after a certain threshold. The classical implementation quickly reaches the maximum number of overlapping cells saturating the performance, therefore further users can only be accommodated by multiplexing them in time, spreading the same summed throughput over an increasing number of users. Analogously, Fig. 5(b) shows the comparison in terms of average user throughput. Also in this case, the performance of the distributed implementations overcomes the classical implementation. For the same reasons previously explained, the performance gap between distributed and classical implementations reduces with the increase of the number of users.

Fig. 5(c) shows the results in terms of throughput density. The distributed implementations provide performance from a few Mbps/km^2 to tens of Kbps/km^2, while classical implementation quickly saturates to few Kbps/km^2. Focusing on the performance of the distributed implementations, the d-URA always slightly overcomes the d-ELSA even if grating lobes are present. It presents a narrower main beam compared to the d-ELSA, and it alternates regions of the beam pattern with high interference (grating lobes) and larger regions with low interference. The d-ELSA mitigates the grating lobe by spreading the interference in all the other parts of the beam pattern instead (Fig. 4). When users are uniformly distributed in the service area, it is more probable that they are generated in the larger area with lower interference than in the smaller area impacted by the grating lobes. Nevertheless, the impact of the grating lobes can be visualized considering the worst-case analysis of the user throughput shown in Fig. 5(d). The d-ELSA overcomes the d-URA for most of the curve. As the number of users increases the number of allocated beams and the average level of interference increases and becomes comparable to the grating lobes level, so after a certain threshold the performance becomes equivalent.

IV. Conclusion

This paper compares the multi-beam performance between classical and distributed implementations of the space segment. Distributed implementations outperform the classical ones in terms of average summed throughput, user throughput, and throughput density. An analysis of worst-case user throughput reveals that distributed implementations based on irregular geometries capable of mitigating grating lobes (d-ELSA) provide slightly lower average performance, but greater fairness than the implementation based on regular geometries (d-URA). This paper compares the results using a simple beamforming scheme, but the upper bound provided shows ample room for improvement. Future works will investigate advanced distributed beamforming schemes to improve performance while maintaining a low complexity.

References

[1] A. Guidotti *et al.*, "The path to 5G-Advanced and 6G Non-Terrestrial Network systems," in *2022 11th Advanced Satellite Multimedia Systems Conference and the 17th Signal Processing for Space Communications Workshop (ASMS/SPSC)*, 2022.

[2] T. Delamotte *et al.*, "Multi-Antenna-Enabled 6G Satellite Systems: Roadmap, Challenges and Opportunities," in *WSA 2021; 25th International ITG Workshop on Smart Antennas*, 2021.

[3] L. Laursen, "No More "No Service": Cellphones will increasingly text via satellite," *IEEE Spectrum*, vol. 60, no. 1, pp. 52–55, 2023.

[4] A. Avellan and Jayasimha Sriram, "System And Method For High Throughput Fractionated Satellites (HTFS) For Direct Connectivity To And From End User Devices And Terminals Using Flight Formations Of Small Or Very Small Satellites," US Patent 9 973 266 B1, May, 2018.

[5] G.-P. Liu and S. Zhang, "A Survey on Formation Control of Small Satellites," *Proceedings of the IEEE*, vol. 106, no. 3, pp. 440–457, 2018.

[6] S. Bandyopadhyay *et al.*, "A Review of Impending Small Satellite Formation Flying Missions," in *53rd AIAA Aerospace Sciences Meeting*, 2015.

[7] K. Alremeithi, J. Miranda Dias, and G. de Masi, "Realization of Pattern Formation For Micro-satellite Swarms Without a Centralized Coordination," in *2022 IEEE International Symposium on Robotic and Sensors Environments (ROSE)*, 2022.

[8] F. Namin, J. S. Petko, and D. H. Werner, "Analysis and Design Optimization of Robust Aperiodic Micro-UAV Swarm-Based Antenna Arrays," *IEEE Transactions on Antennas and Propagation*, vol. 60, no. 5, pp. 2295–2308, 2012.

[9] Solar Power from Space: First Launch on a SpaceX Falcon 9 - IEEE Spectrum. Accessed: Apr. 4, 2023. [Online]. Available: https://spectrum.ieee.org/solar-power

[10] M. Y. Abdelsadek, G. K. Kurt, and H. Yanikomeroglu, "Distributed massive MIMO for LEO satellite networks," *IEEE Open Journal of the Communications Society*, vol. 3, pp. 2162–2177, 2022.

[11] R. Deng, B. Di, and L. Song, "Ultra-dense LEO satellite based formation flying," *IEEE Transactions on Communications*, vol. 69, no. 5, pp. 3091–3105, 2021.

[12] M. Röper *et al.*, "Beamspace MIMO for satellite swarms," in *IEEE Wireless Communications and Networking Conference (WCNC)*, 2022.

[13] M. Y. Abdelsadek *et al.*, "Broadband Connectivity for Handheld Devices via LEO Satellites: Is Distributed Massive MIMO the Answer?" *IEEE Open Journal of the Communications Society*, vol. 4, pp. 713–726, 2023.

[14] G. Bacci *et al.*, "Formation-of-Arrays Antenna Technology for High-Throughput Mobile Non-Terrestrial Networks," *IEEE Transactions on Aerospace and Electronic Systems*, 2023, early access.

[15] D. Tuzi, T. Delamotte, and A. Knopp, "Beamforming performance of satellite swarm-based antenna arrays for 6G direct-to-cell connectivity," in *26th International ITG Workshop on Smart Antennas and 13th Conference on Systems, Communications, and Coding (WSA & SCC 2023)*, 2023.

[16] ——, "Satellite Swarm-Based Antenna Arrays for 6G Direct-to-Cell Connectivity," *IEEE Access*, vol. 11, pp. 36 907–36 928, 2023.

[17] Y. Rahmat-Samii *et al.*, "Realizable feed-element patterns for multibeam reflector antenna analysis," *IEEE Transactions on Antennas and Propagation*, vol. 29, no. 6, pp. 961–963, 1981.

[18] D. Boeringer, "Phased array including a logarithmic spiral lattice of uniformly spaced radiating and receiving elements," US Patent 6 433 754 B1, Apr., 2002.

[19] M. C. Viganó *et al.*, "Sunflower Array Antenna with Adjustable Density Taper," *International Journal of Antennas and Propagation*, vol. 2009, Jan. 2009.

[20] W. C. Y. Lee, *Mobile cellular telecommunications: analog and digital systems*, 2nd ed. New York: McGraw-Hill, 1995.

[21] E. W. Weisstein. Disk Point Picking. Accessed: Jul. 17, 2023. [Online]. Available: https://mathworld.wolfram.com/

[22] T. Lo, "Maximum ratio transmission," *IEEE Transactions on Communications*, vol. 47, no. 10, pp. 1458–1461, Oct. 1999.

[23] W. Yu and T. Lan, "Transmitter Optimization for the Multi-Antenna Downlink With Per-Antenna Power Constraints," *IEEE Transactions on Signal Processing*, vol. 55, no. 6, pp. 2646–2660, Jun. 2007.

[24] P. Angeletti and R. De Gaudenzi, "A Pragmatic Approach to Massive MIMO for Broadband Communication Satellites," *IEEE Access*, vol. 8, pp. 132 212–132 236, 2020.

[25] EnduroSat. 1U CubeSat Platform - Cubesat Platforms. Accessed: Jul. 17, 2023. [Online]. Available: https://www.endurosat.com/cubesat-store/cubesat-platforms/1u-cubesat-platform/

[26] 3GPP, "5G; NR; User Equipment (UE) radio transmission and reception; Part 5: Satellite access Radio Frequency (RF) and performance requirements," 3GPP, Technical Specification (TS) 38.101-5, 04 2023.